Bond performance of FRP bar reinforced concrete under monotonic load and Fatigue effect

Bin Cai [1], Jun Tong [2], Feng Fu [3*]

Bin Cai PhD
Professor, School of Civil Engineering, Jilin Jianzhu University, Changchun, Jilin, PR China
Jun Tong BSc
Master's student, School of Civil Engineering, Jilin Jianzhu University, Changchun, Jilin, PR China
Feng Fu PhD, MBA, FICE
Senior Lecturer, Department of Engineering, School of Science and Technology, City, University of London, London, UK (corresponding author: feng.fu.1@city.ac.uk)

Abstract

In order to investigate the bonding properties of FRP-reinforced concrete under different loads, a series of FRP-reinforced concrete specimens were subjected to pull-out tests. Three types of reinforcement were used in the experiment: ordinary steel reinforcement, carbon fiber reinforcement (CFRP), and glass fiber reinforcement (GFRP). Pull-out tests were first conducted under monotonic load to determine the effect of concrete strength and reinforcement diameter on the bond performance of FRP bar-reinforced concrete and steel-reinforced concrete. The investigation of the variation of bond performance under different reinforcement materials was made. Second, a fatigue test was done, followed by further pull-out tests to get the bond stress-slip curve between concrete and reinforcement, and the influence of fatigue action on the bond stress-slip curve was further examined. The formulae to calculate the stress were developed, which can be applied to determine the bond failure pattern, bond strength, and bond-slip curve.

Keywords： Fiber-reinforcement; Bond; Fatigue; Bond-slip curve; Monotonic load;

Notation

A_s cross-sectional area of the reinforcement

d diameter of the reinforcement (mm)

E_{f} Modulus of elasticity

E_s modulus of elasticity of the reinforcement

f_{fu} Tensile strength

f_{t} splitting tensile strength of the concrete

l buried length of the reinforcement (mm)

P tension (KN)

w/b	Water/binder ratio
Δl	distance between measurement point i and i+1
ε	strain at the measurement point of the reinforcement
ε_f	Elongation
σ	stress at the measurement point of the reinforcement
α	coefficient (The coefficient α is different for different rebar types)
τ_u	bonding strength

1. Introduction

In practice, the bond strength between reinforcement and concrete influences the mechanical characteristics of reinforced concrete buildings significantly (Huang *et al.*, 2016), and the sufficient bond between the reinforcement and concrete ensures the transferability of stress and good coordination of deformation, thus eliminating the local failure of the structure under design loads(Wu and Chen, 2015; Pothisiri and Panedpojaman, 2012). However, debonding may occur in practice because of insufficient bond strength or embedment length, especially at locations where shear forces are concentrated (Ding *et al.*, 2014). Therefore, investigating bond performance between reinforcement and concrete is one of the most critical issues in the basic theory of reinforced concrete.

In marine construction, the issue of steel reinforcement corrosion in reinforced concrete is significant due to chloride salt attacks, which causes a series of safety problems in the structures. The total cost of reinforced concrete damage loss due to lack of durability caused by reinforcement corrosion is estimated at $2.5 trillion (Broomfield, John P,2023; Bowman *et al.*, 2016). The choice of FRP reinforcement as an alternative material to steel reinforcement in concrete structures can be a good solution (Cosenza *et al.*, 1997; Liu *et al.*, 2017; Aiello *et al.*, 2003; Micelli and Nanni, 2003). As a result, studying the bond performance of FRP-reinforced concrete is critical in engineering practice.

Some reinforced concrete structures, such as industrial buildings and bridges, face fatigue problems during long-term service in real environments due to cyclic loads such as vehicle loads from transportation, impact loads from ocean waves, and wind loads (Shen *et al.*, 2016). It has been shown that cyclical loading leads to the continuous deterioration of bond properties between reinforcement and concrete, which in turn results in larger crack widths and deflections, which will seriously affect the durability performance of reinforced concrete structures. Under fatigue loading, the reinforcement in the bonded zone is subjected to cyclical loading and unloading stresses, and the distribution of bond stresses is constantly changing, leading to accumulation of bond damage, gradual increase in relative slip, reduction in bond stiffness, and decrease in average bond strength, which is collectively referred to as bond degradation. Verna and Stelson (1962) systematically studied various damage modes of reinforced concrete beams under cyclical loading and found that flexural members are most susceptible to bond fatigue damage. Edwards and Yannopoulos (1978), Koch and Balazs (1992,1993), and Lindorf et al. (2009,2010) carried out a series of pull-out tests under cyclical loading. In the 1970s, Morita and Kaku (1979,1973) investigated the influence of cyclical stress on bond performance and linked the bond-slip relationship between reinforcement

and concrete to the formation of microcracks in concrete. They concluded that the slope of the bond stress-slip curve under cyclical loading is decreasing gradually. Therefore, it was determined that cyclical loading reduces bond stiffness. Rehm and Eligehausen (1979) used pull-out tests to study the influence of cyclical loading on the bond performance of deformed reinforcement. They found that after fatigue loading, the slope of the bond-slip curve was steep under static loading, which was thought to be due to fatigue loading's reinforcement of the concrete in front of the rib. Perry (1969) investigated the bond stress distribution under cyclical loading by pull-out tests. The peak bond stress was discovered to be mostly centered on the loaded end and the free end, and when the fatigue number grew, the bond stress steadily increased at the free end and reduced at the loaded end.

According to the preceding literature, In engineering practice, analyzing the bond performance of FRP-reinforced concrete under both monotonic and fatigue loads is extremely useful (Achillides and Pilakoutas, 2004; Benmokrane and Tighiouart, 1996). Fatigue damage accumulation of reinforced concrete structure is an irreversible process, when the damage accumulation exceeds the structural load, the structure will be less than its ultimate load-carrying capacity in the case of fatigue brittle damage. Fatigue damage accumulation is often neglected because of its strong concealment, and fatigue damage is transient, which often leads to catastrophic consequences. The fiber-reinforced concrete under fatigue loading is even more rarely studied. Therefore, it is particularly important to study the deterioration of bond properties of reinforced concrete and fiber-reinforced concrete under fatigue loading. It is important for the correct evaluation of the mechanical properties and durability of the actual engineering structures. It is also of great significance for the correct evaluation of the mechanical properties and durability of the actual engineering structures and is of great significance as a design guide for the future service of reinforced concrete structures in harsh environments. An experimental program of 36 FRP-reinforced specimens was carried out to analyze the failure pattern to fill this gap. The bonding performance between FRP reinforcement and concrete under monotonic and cyclical loading was investigated. Based on considering concrete strength, rebar diameter, and rebar material type, bond-slip curves, and bond stress distribution laws were established.

2. Experimental program

2.1 Materials

The cement used for this test specimen is ordinary silicate cement of grade 42.5; coarse aggregate is crushed stone of continuous grain size with a maximum aggregate diameter of 12mm; sand is natural river sand (medium sand) with mud content, not more than 2%; mixing water is tap water. Table 1 shows the test block's fitting ratio.

Table 1. Characteristics properties of concrete

grade	w/b	Water（kg/m^3)	Cement（kg/m^3)	Sand（kg/m^3)	Stone（kg/m^3)
C30	0.56	207	370	721	1127
C40	0.42	202	480	572	1111
C50	0.45	223	496	606	1297

w/b = Water/binder ratio

Table 2. Strength of concrete

Concrete design grade	Compressive strength of concrete（MPa）	Tensile strength of concrete（MPa）

C30	32.83	2.66
C40	42.45	3.30
C50	54.56	3.73

In this paper, six groups of concrete cube specimens were made considering different strength classes of concrete, three groups of concrete specimen blocks were used for concrete compressive strength test and three groups of concrete specimen blocks were used for concrete tensile strength. Three specimens under the same conditions were taken as a group and the results of three tests in each group were averaged. The dimensions of the concrete cubes are 150mm×150mm×150mm for measuring the actual concrete compressive strength and concrete tensile strength. The test results are shown in Table 2.

Existing research indicates that the bonding strength between FRP bars with flat surfaces and concrete is quite low (Tighiouart *et al.*, 1998). Therefore, the FRP bars used in this paper are deformed bars with "ribs" on the surface of FRP bars.

Three types of reinforcement were used in the experiment, namely ordinary steel reinforcement, carbon fiber reinforcement (CFRP), and glass fiber reinforcement (GFRP) (see Figure 1). A steel tube with a 20 mm inner diameter, 1 mm wall thickness, and 150 mm length was fabricated for the test. Epoxy resin was filled to anchor it at both ends of the reinforcement material so that the reinforcement material could be tested in tension on the tensile device.

(a) **(b)** **(c)**

Figure 1. Reinforcement types Type. **(a)** Ordinary steel reinforcement **(b)**Carbon Fiber Reinforcement**(c)**Glass fiber reinforcement

The strength of the steel bars used is HRB400. The rib height of a rebar is approximately 0.1 times the bar diameter, the rib spacing of a 10mm bar is approximately 0.7 times the bar diameter, and the rib spacing of a 12mm bar is approximately 0.8 times the bar diameter. The rib height of the composite fiber reinforcement is approximately 0.03 times the reinforcement diameter, and the rib spacing is approximately 0.3 times the reinforcement diameter. The FRP reinforcement material's tensile strength and ultimate tensile strain were measured using the mechanical indexes given by Harbin FRP Research Institute, see Table 3.

Table 3. Mechanical properties of FRP rebar

FRP tendon type	f_{fu} (MPa)	E_f (GPa)	ε_f (%)
GFRP	1125	45	2.5
CFRP	1920	128	1.5

f_{fu} - Tensile strength； E_f - Modulus of elasticity； ε_f - Elongation

2.2 Test specimens

According to the requirement of the "Concrete Structure Test Method Standard" (GB50152-92), the concrete cube specimen with a side length ten times the diameter of the reinforcement was used to pull out the sample, so in the bond test of FRP bars and concrete, a 150mm×150mm×150mm mold was chosen. A round hole of 20mm in diameter was punched in the middle of both sides of the mold so that the PVC pipes set at the ends of the bars could be penetrated. Before the specimen was fabricated, the sample's embedded length was determined. PVC long hard plastic sleeves were placed at both the free end and the loaded end to isolate the bond between the FRP bars and the concrete to control the anchorage length of the bars and also to avoid the local extrusion damage of the concrete caused by the large load at the loaded end. Since the diameters of the tendons vary, there is a certain difference with the diameter of the PVC sleeve, so the diameter is increased by winding gauze at the location of the free end and loading end of the tendons so that the PVC pipe can be fixed firmly, as shown in Figure 2.

(a) **(b)**

Figure 2. Test piece fabrication (a)FRP tendon production(b)Reinforced concrete specimen.

A total of 36 reinforced concrete bond specimens were produced for this test. Among them, three concrete strengths, three reinforcement types, two rebar diameters, and two loading methods (monotonic and cyclical loading method), where the anchorage length of the reinforcement is set at 5d (d is the diameter of the reinforcement), and the experiment is divided into two groups for experimental study, monotonic load group, and preloaded fatigue load group. The specific parameters of the specimens were set, as shown in Tables 4 and 5.

Table 4. Monotonic load group specimen-specific parameters setting

Specimen number	d	Materials	Concrete strength	Loading method	Number
C-C30-10	10	CFRP	C30	Monotonic loading	1
C-C40-10			C40	Monotonic loading	1
C-C50-10			C50	Monotonic loading	1
C-C30-12	12		C30	Monotonic loading	1
C-C40-12			C40	Monotonic loading	1
C-C50-12			C50	Monotonic loading	1
G-C30-10	10	GFRP	C30	Monotonic loading	1

G-C40-10			C40	Monotonic loading	1
G-C50-10			C50	Monotonic loading	1
G-C30-12			C30	Monotonic loading	1
G-C40-12	12		C40	Monotonic loading	1
G-C50-12			C50	Monotonic loading	1
N-C30-10			C30	Monotonic loading	1
N-C40-10	10		C40	Monotonic loading	1
N-C50-10		Rebar	C50	Monotonic loading	1
N-C30-12			C30	Monotonic loading	1
N-C40-12	12		C40	Monotonic loading	1
N-C50-12			C50	Monotonic loading	1

Table 5. Specific parameter setting for the specimen of preloaded fatigue load group

Specimen number	*d*	Materials	Concrete strength	Loading method	Number
PC-C30-10			C30	Fatigue loading	1
PC-C40-10	10		C40	Fatigue loading	1
PC-C50-10		CFRP	C50	Fatigue loading	1
PC-C30-12			C30	Fatigue loading	1
PC-C40-12	12		C40	Fatigue loading	1
PC-C50-12			C50	Fatigue loading	1
PG-C30-10			C30	Fatigue loading	1
PG-C40-10	10		C40	Fatigue loading	1
PG-C50-10		GFRP	C50	Fatigue loading	1
PG-C30-12			C30	Fatigue loading	1
PG-C40-12	12		C40	Fatigue loading	1
PG-C50-12			C50	Fatigue loading	1
PN-C30-10			C30	Fatigue loading	1
PN-C40-10	10		C40	Fatigue loading	1
PN-C50-10		Rebar	C50	Fatigue loading	1
PN-C30-12			C30	Fatigue loading	1
PN-C40-12	12		C40	Fatigue loading	1
PN-C50-12			C50	Fatigue loading	1

Thirty-six reinforced concrete blocks were correspondingly made, and PVC sleeves were buried at the end of the specimens, designed as a bond-free zone. The specimen numbers are A-B-C. A represents the reinforcing material (C represents CFRP reinforcement-concrete specimen, G represents GFRP reinforcement-concrete specimen, N represents steel reinforcement-concrete specimen), B represents concrete strength, and C represents reinforcement diameter.

Before the concrete is poured, grooves are cut in the surface of the reinforcement, and strain gauges are uniformly pasted inside the grooves to obtain an accurate strain distribution of the reinforcement under load. Six strain gauges were arranged at an interval of 10 mm in the bonded section of the reinforcement, and air bubbles were removed from the contact surface to ensure that the strain gauges firmly adhered to the reinforcement. After all strain gauges are pasted, the two external wires of the strain gauges are soldered to the enameled wire of 0.25mm diameter, as shown in Figure 3.

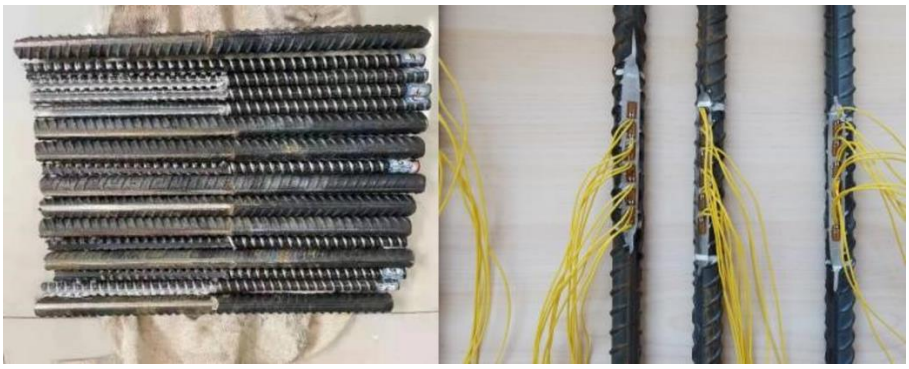

(a) **(b)**

Figure 3. Steel treatment (a)Steel surface grooving (b)Applying strain gauges

2.3 Loading regimes

Figure 4 depicts the pull-out test setup. A steel frame consisting of two steel plates of 30 mm thickness and five steel bars with a diameter of 25 mm is used to restrain each specimen. The upper clamp of the universal testing machine clamps the steel bar fixed in the center of the top steel plate. The bottom fixture clamps the specimen's reinforcement through pre-drilled holes in the base plate. During the pull-out test, lubricant is applied between the test block and the bottom plate to reduce friction between the test piece and the steel plate. Two displacement gauges are attached to the test block's top to detect the relative displacement of the reinforcement and the test block, and the tensile force is determined by the universal testing machine's force measurement device. The bond strength of the reinforced concrete was obtained by equation (1).

$$\tau = \frac{P}{\pi dl} \tag{1}$$

Where: P is the tension (KN), d is the diameter of the reinforcement (mm), l is the buried length of the reinforcement (mm)

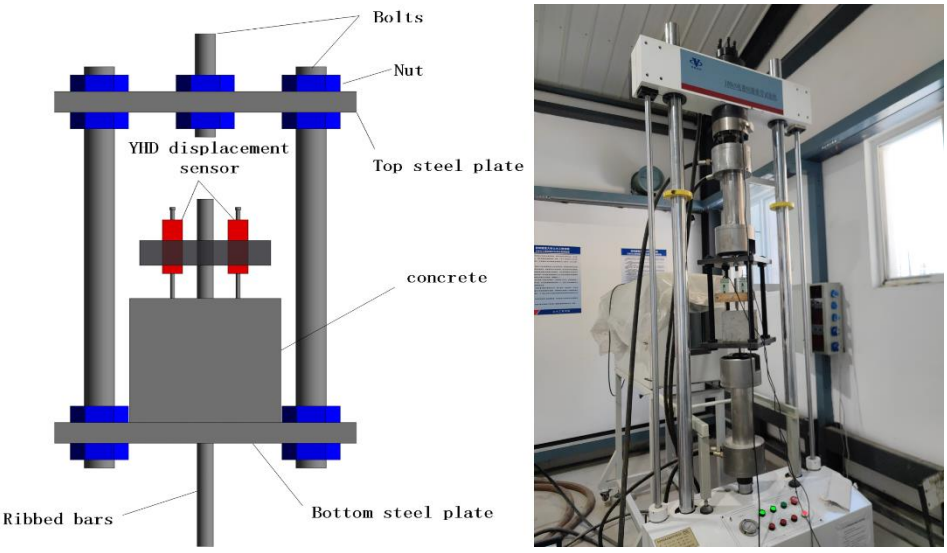

(a) Pull-out test device **(b)** Fatigue testing machine

Figure 4. Pull-out test setup

Different loading methods were adopted for the two groups of test blocks.

Monotonic loading: The displacement control is used. Moreover, the load rate is 0.5 mm/min until the pull-out displacement is 4 mm when the loading is stopped. Compared with load control,

displacement control can better monitor the slipping between the steel reinforcement and concrete. Pay attention to the change of specimen on the testing machine at any time, record the specimen's load-displacement curve when it reaches the peak load, record the displacement count value when it reaches the peak load, and continue to load until the relative displacement between the reinforcement and concrete reaches 4 mm, or the specimen is damaged, and terminate the test.

Cyclical loading: Firstly, the load was increased step by step to the upper limit of the cyclical load (P_{max}=45%P) and then decreased step by step to the middle value of the upper load limit and lower load limit (P_{min}=10%P) for repeated loading. The loading frequency of the specimen with 10,000 fatigue cycles was 4 Hz.

After reaching the set number of repetitive loading, the monotonic load was continued to be used for the specimen at a loading rate of 0.5 mm/min until the specimen was damaged. After the cyclical loading test, some specimens were found to have fine cracks at the bottom, mainly due to fatigue loading.

3. Test phenomenon and results

3.1 Monotonic loading

3.1.1 Failure mode

In this standard pull-out test, a total of 18 standard specimens were loaded with a controlled loading speed of 0.5mm/min. When one of the following three phenomena occurred in the specimens, we decided that the specimens had been damaged, stopped loading, and recorded the experimental data. ①The concrete specimen is damaged by splitting. ②Slip value of the free end exceeds 20mm. ③Fracture of GFRP reinforcement occurs. ④The load value dropped to 70% of the ultimate load value and did not tend to rise again.

The damage to the specimens includes the pull-out damage of GFRP tendons and the concrete splitting damage. In the tendon pull-out, damage includes the shearing of the rib and the shearing of the concrete between the ribs. The damage patterns are shown in Figure 5.

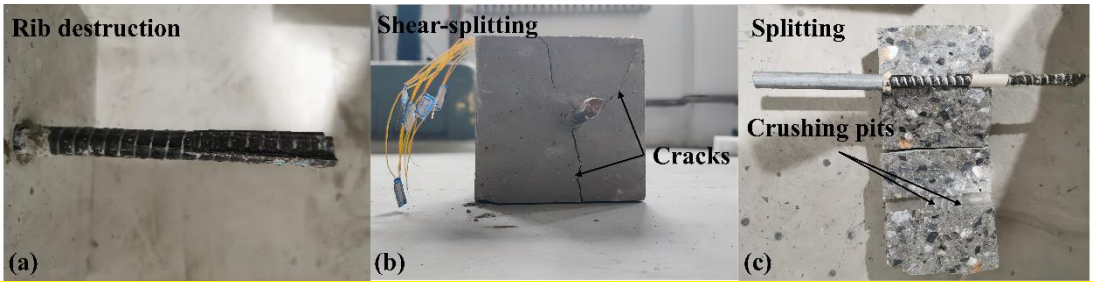

Figure 5. Tensile test damage mode

In this test, rib pull-out damage was observed in many specimens, and the specific results are shown in Table 6. Rib stripping pull-out damage was characterized by an increase in the slip at the loading end along with the test process, and the FRP bars slowly pulled out, eventually leading to damage without splintering of the concrete and fracture of the FRP bars. For the specimen with such damage, the cross ribs on the surface of the FRP bars were sheared off by the concrete when the FRP bars were pulled out, resulting in a large slip, and the surface of the FRP bars around the concrete hole wall had been basically worn flat and damaged due to the longitudinal abrasion. The thicker concrete protective layer and the smaller diameter of FRP bars or the lower height of the cross ribs cause this damage. This kind of damage belongs to bond damage; the damage form is

shown in Figure 5(a).

Shear-splitting damage refers to a phenomenon wherein the reinforcement is exposed to pulling forces, which results in reinforcement extraction from the surrounding material. Notably, the test block exhibits cohesive behavior in such instances, maintaining its integrity as a single entity. Nevertheless, careful observation, as illustrated in Figure 5(b), reveals the existence of discernible microcracks predominantly localized at the lower region of the test block.

One type of pull-out damage is caused by low concrete strength or short bond length, which is summarised in this paper as inter-rib concrete splitting damage. The surface phenomenon of this damage is the same as the rib-stripped reinforcement pull-out damage, but the internal damage mechanism is different. The reason for this damage is that during the loading process, the concrete strength at the interface between the FRP reinforcement and the concrete bond is insufficient, and splitting will occur under a specific load, and this damage spreads from the loading end to the free end, eventually leading to reinforcement pull-out and specimen damage, as shown in Figure 5(c).

Reinforced concrete test blocks are mostly subjected to splitting, splitting, and pull-out damage.

Table 6. Summary of failure modes of the tested specimens.

Specimen number	Monotonic loading
C-10-C30	Splitting
C-10-C40	Splitting
C-10-C50	Rib destruction
C-12-C30	Splitting
C-12-C40	Splitting
C-12-C50	Rib destruction
G-10-C30	Splitting
G-10-C40	Splitting
G-10-C50	Rib destruction
G-12-C30	Splitting
G-12-C40	Splitting
G-12-C50	Splitting
N-10-C30	Shear-splitting
N-10-C40	Splitting
N-10-C50	Splitting
N-12-C30	Shear-splitting
N-12-C40	Splitting
N-12-C50	Splitting

3.1.2 Bond-slip relationship

Since the test conditions of each group of specimens vary, there will be many bond-slip curves obtained, totaling 18 bond-slip curves, as shown in Figure 6. The displacements in the Figures start from the application of load to the destruction of the specimen. Since the loaded end bars will break and destroy during the loading process, some specimens do not measure the displacement of the falling section when they reach destruction.

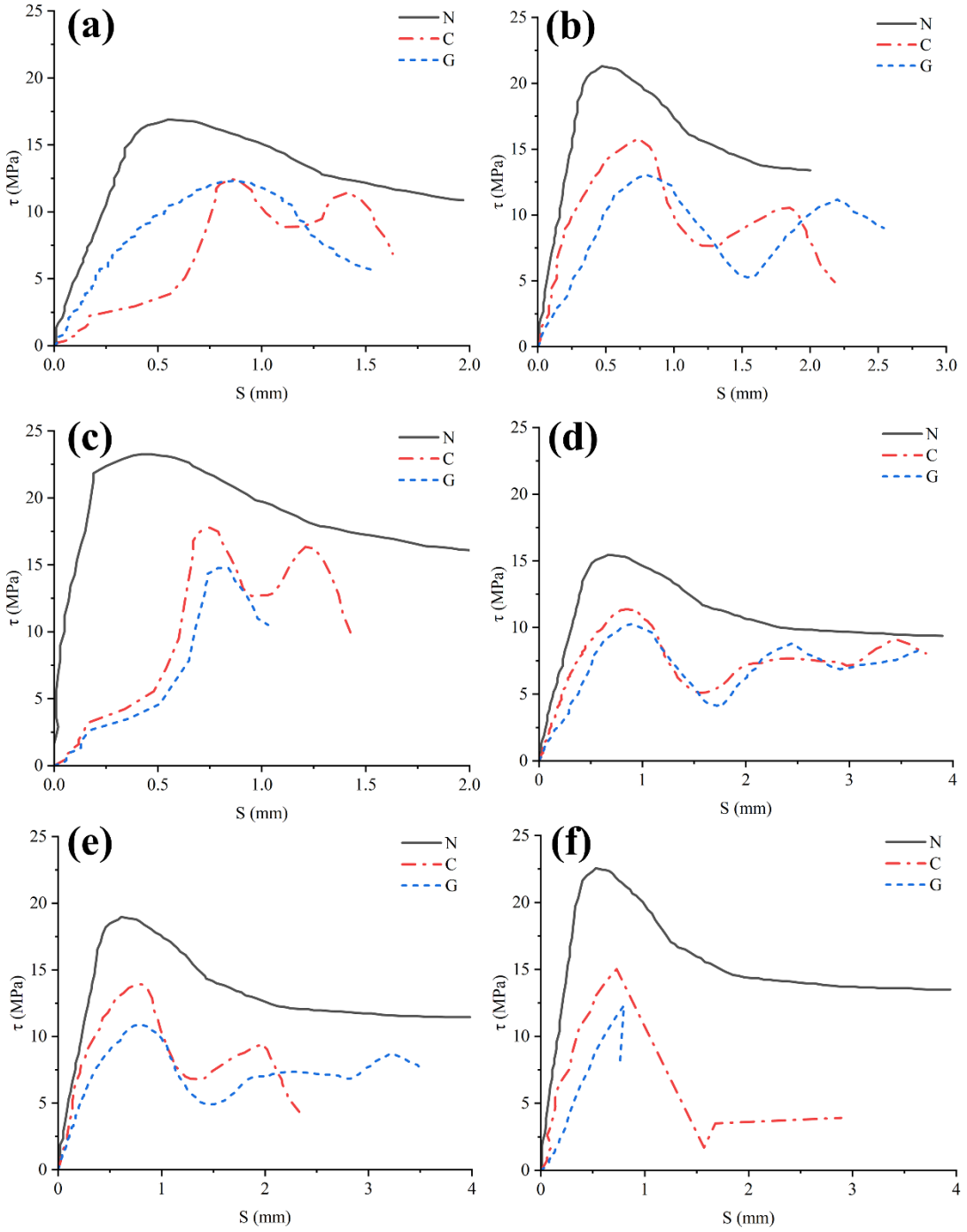

Figure 6. Bond-slip curves of different reinforcement materials:(a)C30-10(b)C40-10(c)C50-10(d)C30-12(e)C40-12(f)C50-12

By analyzing these bond-slip curves, it can be concluded that most of the specimens have residual stresses in their bond-slip curves, except for the specimen with no descending section in Figure 6. For the residual stress stage, the bond stress fluctuates and may produce a second small peak as well as a third small peak so that the bond-slip curve can be broadly divided into three sections: rising section, falling section, and residual stress stage. The bonding process of the specimen is classified into the following stages.

(1) Microslip phase

The FRP tendon was in the early stages of pull-out at the start of the test. The slip at the loading end was modest at this point. The tendon at the free end had not slipped, and the curve was in the linear elastic stage. The chemical adhesive force between the FRP bars and the concrete is broken as the load increases from the loading end to the free end, and the slide steadily stretches to the free end, but it has not yet reached the free end. This is not the same as the bond-slip curve between steel and concrete. Moreover, since the height and width of the "ribs" of each FRP bar are different, the amount of micro-slip is also different, and the load value at the beginning of the slip at the free end is also different. During this phase, the slip at the loaded end also includes the elastic elongation of the FRP tendons on the exposed side of the loaded end, which has been set to minimize the error by deleting individual points in the data-gathering system during the test.

(2) Slip phase

As the load increases, the bonded interface near the loading end begins to show local debonding. The debonding surface gradually develops from the loading end to the free end, and the slip at the loading end increases rapidly. At the same time, the slip at the free end also begins to produce slip, indicating that the chemical adhesive force between FRP bars and concrete has entirely lost the bonded slip. The bond stress between FRP bars and concrete is mostly formed by the mechanical bite force between the projecting ribs on the surface of the bars and the concrete, as well as the friction force at the bond interface.

(3) Pull-out stage

When the load was increased further, the non-linearity of the bond-slip curve became clear. At the moment, the relative slip between the FRP rib and the concrete increased more quickly, but the load value gradually increased, and the slope of the curve steadily decreased, but the turn was not obvious. Because of the thick concrete protection layer, there was no visible crack on the surface of the specimen during the test, and the mechanical bite between the rib and the concrete was partially but not damaged from the loaded end to the free end. The binding tension between FRP rib and concrete was still composed of mechanical biting and interfacial friction forces. Furthermore, when the bond stress reaches its peak, it does not keep a constant value at the peak, as in the case of the bond-slip curve of reinforced concrete, but it rapidly decreases.

(4) Decline phase

When the load approaches its maximum value, the slip at the loaded and free ends increases dramatically while the load value falls dramatically. The mechanical bite and interfacial friction between the FRP bars and the concrete are largely dissolved, the bonding effect becomes increasingly weak, and the bars are gradually dragged out of the concrete's center.

(5) Residual fluctuation phase

When the load is reduced to a certain level, the bond-slip curve rises and enters the stress-residual phase. The graph shows that bond stress will climb back to the second minor peak, then decline and increase again, repeated several times until the FRP tendons are completely pulled out from the concrete. For this occurrence, the reason is that when the interfacial bond stress is broken, there will be concrete residue stuck on the FRP tendons, or the next intact rib remaining will raise the unevenness of the interface, and when the displacement increases, there may be weak mechanical occlusion phenomenon and interfacial friction phenomenon, which makes the curve -s have residual fluctuation section. Therefore, the binding tensions between FRP bars and concrete are still mechanical occlusion and interfacial friction at this stage.

Table 7. Strength Summary Table under Monotonic Loading (MPa).

Specimen number	C30		C40		C50	
	Bonding stress	Peak slip	Bonding stress	Peak slip	Bonding stress	Peak slip
C-10	12.43	0.83	15.71	0.72	17.80	0.74
C-12	11.35	0.87	13.94	0.77	15.02	0.73
G-10	12.3	0.88	13.03	0.80	14.77	0.79
G-12	10.25	0.89	10.86	0.81	12.31	0.80
N-10	16.9	0.55	21.3	0.47	23.26	0.42
N-12	15.46	0.67	18.97	0.61	22.56	0.53

The typical curves in the two groups of specimens were selected for comparison. The concrete strength was C30, the bond length was 60mm, the bar diameter was 12mm, and the bond damage on both the CFRP and GFRP bar specimens was pull-out damage. When the bond-slip curves were compared, the following results were reached.

(1) The bond-slip curves of CFRP reinforcement are depicted in Figure 6(d). The bond-slip between GFRP reinforcement and concrete has much in common with the bond-slip between steel and concrete: the bond-slip stages of both can be broadly divided into micro-slip, slip, pull-out, drop, and residual stress fluctuation sections.

(2) Figure 6(d) shows that, under the same external conditions, the maximum bond strength of CFRP reinforcement to concrete is greater than that of GFRP reinforcement to concrete. This is because the fibers contained in CFRP reinforcement are carbon fibers, and the tensile strength of this fiber is greater than that of glass fiber, resulting in the "rib" formed on the surface of the reinforcement. As a result, the tensile and compressive strength of the "rib" generated on the surface of the reinforcement will be greater than that of the GFRP reinforcement, significantly improving mechanical bite between the FRP reinforcement and the concrete and thereby enhancing bond strength.

(3) As can be seen from Figure 6(d), the slope of the CFRP reinforcement's rising region of the bond-slip curve is greater than that of the GFRP reinforcement. This is also owing to the fact that carbon fiber has a higher tensile strength and modulus of elasticity than glass fiber.

(4) As shown in Figure 6(d), when the peak bond stress is attained, the relative slips of CFRP reinforcement and concrete are smaller than those of GFRP reinforcement, indicating that CFRP reinforcement and concrete have higher bonding performance.

3.1.3 Statistical regression analysis

The anchoring force is separated into five phases in the above load-slip (τ-s) curve: micro-slip section (0-s), slip section (s-cr), splitting section (cr-u), falling section (u-r), and residual section (r-). From the critical turning point of the curve, four characteristic strengths of bonded anchorage can be defined: slip strength τ_s, splitting strength τ_{cr}, ultimate strength τ_u, and residual strength τ_r. The corresponding characteristic slip values are s_s, s_{cr}, s_u, and s_r. The splitting cracks are mostly axially injected, and the main cracks occur at the thinnest part of the protective layer. The wedge-like accumulation of crushed concrete in front of the cross rib of the reinforcement. The bite teeth visible from the extracted anchor bars were cut off, the inter-rib was filled with crushed debris, and scuff marks were left on the inner hole wall. The test showed that the bonded anchorage strength increased with the concrete strength f_{cu}, but not linearly, and was proportional to its tensile strength $f_t = 0.26 f_{cu}^{2/3}$. The splitting strength τ_{cr} increases as the protective layer thickness c/d increases.

The diameter of the anchor bar has little effect on τ, while it has a significant impact on slip s, which is roughly proportional, reflecting the effect of inter-rib bite teeth on deformation.

In this study, we utilize the adhesive strength model introduced by Xu Youlin (1988), which has been widely recognized in the field. As the test did not incorporate hoop reinforcement, the influence of hoop reinforcement on the adhesive strength was adjusted to reflect the contribution of concrete alone. Specifically, when $\rho_{sv}=0$, Equation (2) is applied, indicating the scenario where no hoop reinforcement is present. The splitting tensile strength ft is taken according to Table 2.

In this study, we utilize the coefficient of determination R squared (R^2) to evaluate the ability of commonly used interface models to capture experimental results. The coefficient of determination, denoted as R^2, quantifies the extent to which the independent variable accounts for the dependent variable via the regression relationship. An R-squared value of 0.8, for example, indicates that the regression connection accounts for 80% of the variability in the dependent variable. In other words, the dependent variable's variance will decrease by 80% if the control independent variable stays the same.

The bonded anchorage strength of the specimens is shown in Equation (1) by statistical analysis of the test results and verified by tests. The corresponding characteristic slip values are shown in Table 8.

Table 8. Characteristic Slip Value

Type of reinforcement	S_u
Ordinary rebar	0.0542d
Carbon fiber rebar	0.0776d
Fiberglass rebar	0.0828d

$$\tau_u = \left(1.6 + 0.7\frac{c}{d}\right) f_t \alpha \tag{2}$$

Where τ_u represents the bonding strength in units of MPa, the protective layer thickness is denoted by c, the diameter of the bar is denoted by d, and the splitting tensile strength of the concrete is denoted by f_t. α is a coefficient. (The coefficient α is different for different rebar types)

Here is an example of a reinforced concrete test block with a diameter of 12mm. Three different concrete strengths and three different types of reinforcement are included. The coefficient α is 1.025 and R^2 is 0.9758 for plain reinforced concrete with a diameter of 12 mm, which shows that the results fitted by Eq. 2 differ very little from the test values. The coefficient α of carbon fiber reinforced concrete with a diameter of 12 mm is 0.7213 and R^2 is 0.9483, which shows that the difference between the results fitted by Equation 2 and the experimental values is a little larger. The coefficient α for glass fiber reinforced concrete with a diameter of 12 mm is 0.5948 and R^2 is 0.2365, thus it can be seen that the results fitted by Equation 2 differ greatly from the experimental values.

This formula applies to reinforced concrete test blocks and does not extend to fiber-reinforced concrete test blocks. The strength of the concrete is critical in determining the bonding performance between the reinforcing steel and the concrete matrix in the case of reinforced concrete. Experimental tests have demonstrated that the bond strength is directly proportional to the square root of the concrete's compressive strength or tensile strength. However, it is important to acknowledge that fiber-reinforced polymer (FRP) bars exhibit fundamental differences in material properties compared to steel bars. FRP bars have different surface properties than steel bars, and their modulus of elasticity is only one-fourth that of steel bars. As a result, determining whether the

bond strength between FRP bars and concrete has a linear relationship with the square root of the concrete's compressive strength is difficult. This discrepancy in behavior can be primarily attributed to the distinctions between FRP-reinforced concrete and conventional reinforced concrete concerning the pull-out resistance mechanism and the concrete matrix's role.

The test data from 18 specimens yields an impressive coefficient of determination (R^2) value of 0.92. This high R^2 value indicates a robust correlation between the variables under investigation. The proximity to 1 suggests a high degree of predictability and reliability in the relationship between the variables, further reinforcing the validity of the experimental results.

3.1.4 Distribution of bond stress

The test results show (1) the ultimate load measured by the pressure transducer when the reinforcement and concrete are damaged and (2) the strain value of the reinforcement at each measurement point within the reinforcement's anchorage length corresponding to the load at each level. The strain gauges are named in increasing order from the loaded end to the free end, from 1# to 6#.

The variation curves of strain with load for different reinforcement materials are shown in Figure 7 below.

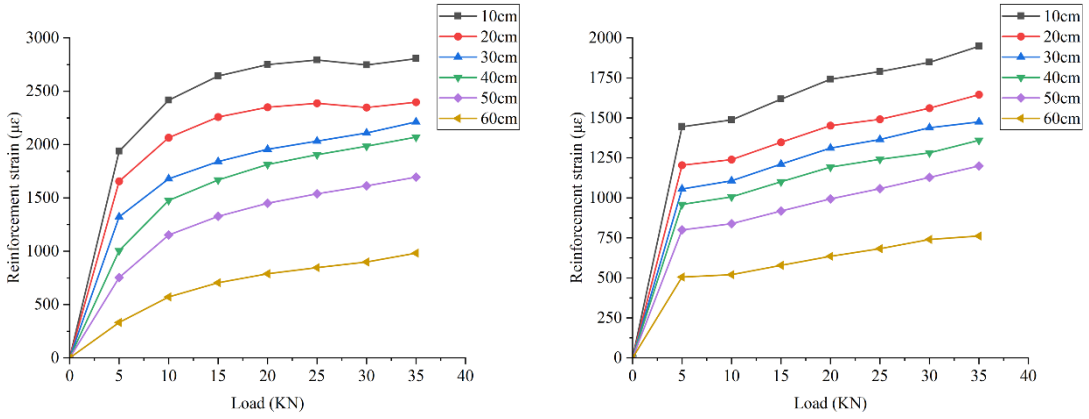

Figure 7. Strain variation curve with load(a)C-C50-10(b)N-C50-10

As seen in Figure 7, the strain of the reinforcement grows as the load increases, implying that the load of the reinforcement is gradually shifted from the loading end to the free end, the relative slip between the reinforcement and the concrete increases, and the bond force between the two gradually decreases. When the load reaches its maximum, the strain of the reinforcement reaches its maximum as well. The main bond between the two relies on the mechanical bite force between the raised rib of the reinforcement and the concrete. No chemical adhesive force is involved in the work, and the curve approximates a straight line. The strain changes linearly with increasing load, and the whole curve has no large inflection point, which means that the reinforcement has not yet reached the yielding stage and the whole bond-slip process is in the elastic stage. Comparing graphs 7(a) and 7(b), the strain of carbon fiber reinforcement is greater than that of steel reinforcement.

The variation curves of reinforcement strain along the anchorage length for different reinforcement materials are shown in Figure 8 below.

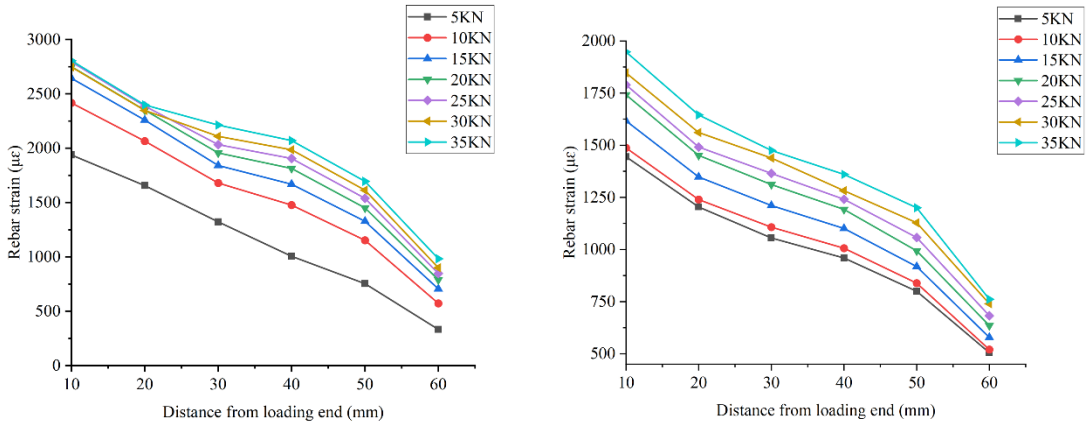

Figure 8. Strain variation curve along the anchorage length(a)C-C50-10(b)N-C50-10

The strain gradually decreases from the loaded end to the free end along the anchorage length and finally tends to 0. It indicates that the bond stress gradually offsets the pull-out load during the transfer from the loaded end to the free end. The relative slip between the reinforcement and concrete gradually increases with the load increase. In the same anchorage section, when the load is small, the reinforcement strain is also small, and the bond stress is mainly the chemical adhesive force between the reinforcement and concrete. As the load gradually increases, the strain of the reinforcement increases and the two are not in synchronous displacement and begin to produce relative slip. The bond stress mainly depends on the mechanical bite force and friction resistance between the reinforcement and concrete.

The test measured the specimen reinforcement's strain value, and the adhesive stress distribution curve was calculated for each measurement point in the anchorage section, as shown in Figure 9. The adhesive action between concrete and reinforcement can be regarded as a shear force action, which is not evenly distributed along the anchorage length. Due to the limitation of measurement technology and means, it is not possible to directly measure the stresses on the contact surface between the reinforcement and concrete at this stage. The stress and strain of the reinforcement vary along the anchorage length caused by the applied load, and the cohesive stress τ transfers the stress of the reinforcement to the concrete, causing stress and strain in the concrete, which in turn generates relative slip S. The cohesive stress between the reinforcement and concrete is deduced from the measured strain change value of the reinforcement in the test. Taking the steel micro-segment isolated body analysis, according to the force equilibrium, we get:

$$A_s\left(\sigma_s + d\sigma_s\right) - \tau\pi d \cdot dx = A_s\sigma_s \tag{3}$$

Simplifying the Equation, we get the following:

$$\tau = -\frac{A_s d\sigma_s}{\pi d \cdot dx} = -\frac{\sigma_{i+1} - \sigma_i}{4\Delta l} = -\frac{E_s d\left(\varepsilon_{i+1} - \varepsilon_i\right)}{4\Delta l} \tag{4}$$

Where: σ is the stress at the measurement point of the reinforcement, ε is the strain at the measurement point of the reinforcement, Δl is the distance between measurement point i and i+1, E_s is the modulus of elasticity of the reinforcement, and A_s is the cross-sectional area of the reinforcement.

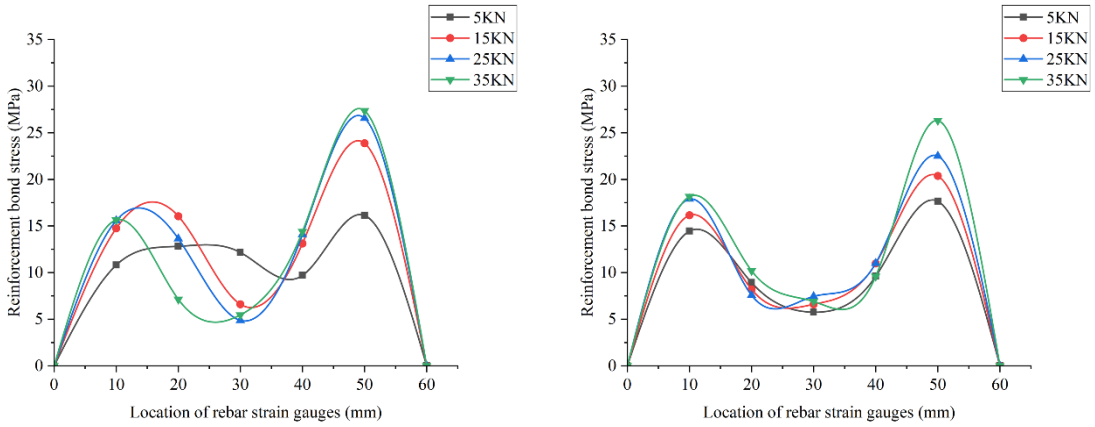

(a) **(b)**

Figure 9. The bond stress distribution curve(a)C-C50-10(b)N-C50-10

As shown in Fig. 9, the bond strength calculated by Eq. 4 in the figure is somewhat different from that calculated by Eq. 1 for the following two reasons: firstly, it should be due to the manual pasting of the strain gauges, which leads to possible errors in the spacing between the strain gauges, and secondly, it is due to the fact that the fibrous reinforcement is broken due to the overstrength of the concrete during the pulling process.

As can be seen in Figure 9, the stress distribution patterns of ordinary steel bars and carbon fiber bars in the bonded section with concrete are "bimodal". With the increase in load, the bond stress near the loading end and the free end increases more, and the increase in the middle part is smaller. The bond stresses near the loaded end and the free end grew faster in the preloading and post-loading periods, respectively, indicating that the location of the bond force gradually shifted from the loaded end to the free end with the increase of the load.

The bond stress was 0 at the specimen's loaded end and free end, and then the bond stress extended from the loaded end to the free end. At the beginning of the test, near the loading end, after the maximum value of the bond stress appears, with the extension of the anchorage position to the free end, the bond stress first decreases and then increases, and the second peak appears, and then gradually decreases to 0, as shown in Figure 9.

3.2 Cyclical loading

3.2.1 Failure mode

In this test, 18 specimens were loaded under cyclical load at a controlled loading rate of 0.5 mm/min. There was no significant difference in the damage mode compared with the monotonically loaded specimens. The damage pattern is shown in Figure 10.

(a) **(b)** **(c)**

Figure 10. Destruction mode(a) Rib destruction(b) Shear-splitting(c) Splitting

(1) Rib destruction

Figure 10(a) illustrates the noticeable effects of fatigue loading on some FRP bar specimens, resulting in evident breakage or flattening of the cross ribs on the surface of the FRP bars. This type of rib destruction directly impacts the bonding performance between the FRP bars and the concrete matrix.

(2) Shear-splitting

The initial state of this type of destruction is the same as that of the splitting destruction at the beginning, except that the test piece of concrete for splitting and extraction destruction did not break into 2-3 samples. The bond-slip curve has a descending segment at this point, and the load decrease is visible to the naked eye. With the continuous increase of external load, the cracks gradually develop, the slip between the steel bar and the concrete increases gradually, and the concrete at the contact position with the steel bar is crushed by the ribs of the steel bar, resulting in penetrating cracks in the specimen. The load slowly decreases and eventually stabilizes. The integrity of the specimen after failure is relatively good. The form of damage is shown in Figure 10 (b).

(3) Concrete splitting damage

Most of the failure cracks in the bonded specimens did not occur in the weak concrete cover but in the form of penetrating cracks located on the diagonal of the concrete, dividing the concrete cover into two parts. The FRP reinforcement traces are clear on the fractured section of the failure specimen, and the surface and ribs of the FRP reinforcement only have slight wear, indicating that there is no obvious slippage between the FRP reinforcement and the concrete of the specimen. It is worth noting that the failure load of the bonded specimen increased significantly, and the failure cracks appeared randomly without obvious regularity. The FRP reinforcement and PVC sheath have no concrete fragments adhered to them. On the fractured section of the failure specimen, in addition to clear traces of FRP reinforcement and ribs, epoxy resin debris left after damage to the reinforcement and a small amount of fiber traces at the mechanical interlocking points of the ribs can be observed. The form of damage is shown in Figure 10 (c).

Table 6. Summary of failure modes of the tested specimens.

Specimen number	Monotonic loading after fatigue loading
C-10-C30	Splitting
C-10-C40	Splitting
C-10-C50	Rib destruction
C-12-C30	Splitting
C-12-C40	Shear-splitting
C-12-C50	Rib destruction
G-10-C30	Splitting
G-10-C40	Splitting
G-10-C50	Rib destruction
G-12-C30	Splitting
G-12-C40	Splitting
G-12-C50	Rib destruction
N-10-C30	Shear-splitting
N-10-C40	Shear-splitting
N-10-C50	Shear-splitting
N-12-C30	Shear-splitting
N-12-C40	Shear-splitting

3.2.2 Bond-slip relationship

Since the test conditions of each group of specimens vary, there will be many kinds of bond-slip curves in the test, and several representative groups of bond-slip curves are selected for study in this paper, as shown in Figure 11. The displacements in the Figure start from the application of load to the destruction of the specimen. Since the loaded end bars will break and destroy during the loading process, some samples do not measure the displacement of the falling section when they reach destruction.

Bond slip curve after fatigue

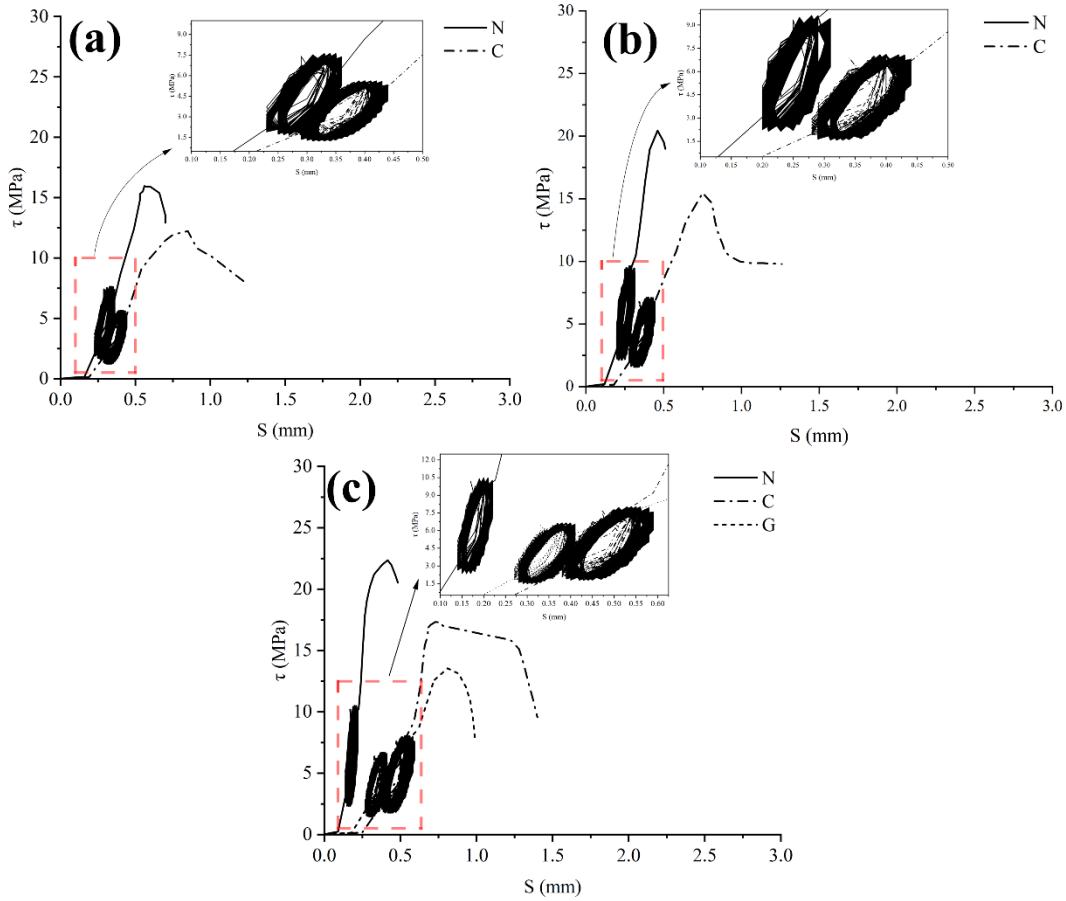

Figure 11. Bond-slip curves of different reinforcement materials after fatigue effect (a)C30-10(b)C40-10(c)C50-10

As shown in Figure 11, comparing monotonically loaded specimens with repeatedly loaded samples, we can see that the bond strength is almost identical under both loading methods, and cyclical loading has no significant effect on the bond strength degradation law.

Table 9. Strength Summary Table under Cyclical loading (MPa).

Specimen number	C30		C40		C50	
	Bonding stress	Peak slip	Bonding stress	Peak slip	Bonding stress	Peak slip
C-10	12.22	0.85	15.47	0.75	17.33	0.73
C-12	11.11	0.88	13.33	0.76	14.87	0.75

G-10	8.55	1.11	9.25	0.98	13.55	0.81
G-12	9.96	0.91	10.21	0.84	11.77	0.79
N-10	15.96	0.56	20.44	0.46	22.36	0.41
N-12	14.98	0.62	18.21	0.60	21.99	0.54

As can be seen in Figure 11, the bond stress-slip curves measured after different repeated loads than the monotonically loaded specimens consist of four parts: the hysteresis loop, the hardening section (rising section), the falling section, and the horizontal section. The hysteresis loop and hardened section are enlarged locally in the Figure. The area of the hysteresis loop increases with increasing load level, indicating that unrecoverable residual relative slip of the reinforcement and concrete occurs under cyclical loading and increases with repeated loads. At the end of the repeated loading, the bond stress increased to a peak and then slowly decreased, similar to the monotonically loaded specimens.

The non-linear characteristics of the rising part of the bond-slip curve (the rising section of the monotonic pull-out after 10,000 fatigue cycles) appeared later than those of the monotonic pull-out loaded specimens, which indicated that the bond stiffness of the specimens improved under the fatigue loading, and the residual bond stress did not change much, which was basically the same as the falling section of the monotonic pull-out curve, indicating that the cyclical loading had no significant effect on the falling area of the monotonic pull-out bond-slip curve. After cyclical loading and continued monotonic loading, the load reached the peak and then decreased, and the bond stress-slip curve characteristics of the specimen at this stage were approximately the same as that of the monotonic loaded sample.

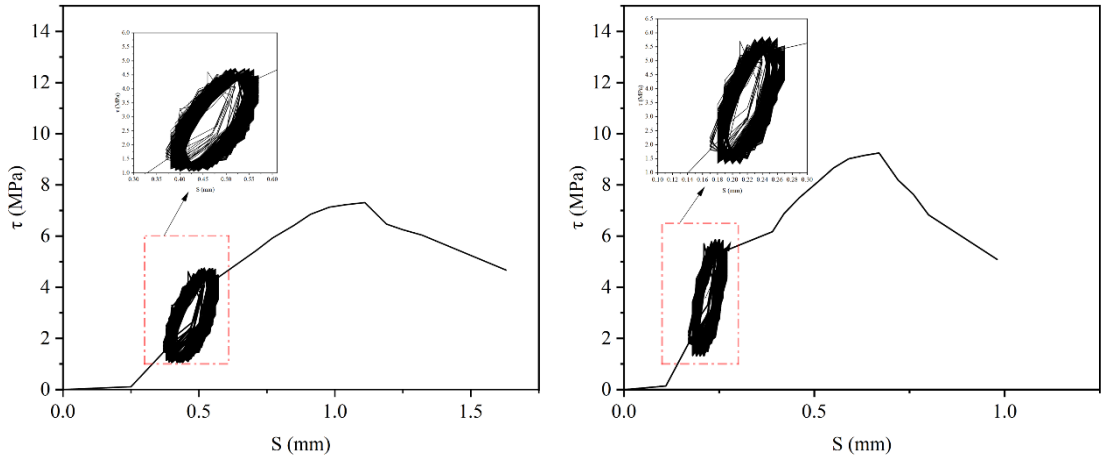

Figure 12. Bond-slip curve after fatigue effect (a)G-10-C30(b)G-10-C40

As depicted in Figure 12, the fatigue loading led to the damage of certain ribs in the fiber reinforcement, resulting in a reduced peak bond stress. The bond mechanism between FRP bars and concrete is analogous to that observed in reinforced concrete, primarily involving chemisorption, friction, and mechanical occlusion forces. However, there are notable distinctions between FRP bars and steel reinforcement. Specifically, FRP bars have lower surface hardness and shear strength when compared to concrete. Consequently, under the influence of fatigue loads, the ribs of FRP bars are more susceptible to damage when compared to steel bars.

4. Effect of different parameters on bond performance after cyclic loading

4.1 Effect of concrete strength on bond strength

Concrete strength is an important factor influencing the bonding performance of reinforcing steel to reinforced concrete. Bond strength is related to the square root of concrete's compressive or tensile strength, according to testing. The material properties of FRP bars, on the other hand, differ greatly from those of steel bars. It's difficult to say if the bond strength of FRP bars is directly proportional to the square root of concrete's compressive strength. Therefore, the effect on the concrete strength still needs a lot of experimental studies. In this paper, this factor is considered, and the design strengths of C30, C40, and C50 are used to examine the effect of concrete strength on the bonding performance of FRP bars, see Figure 13 and Figure 14.

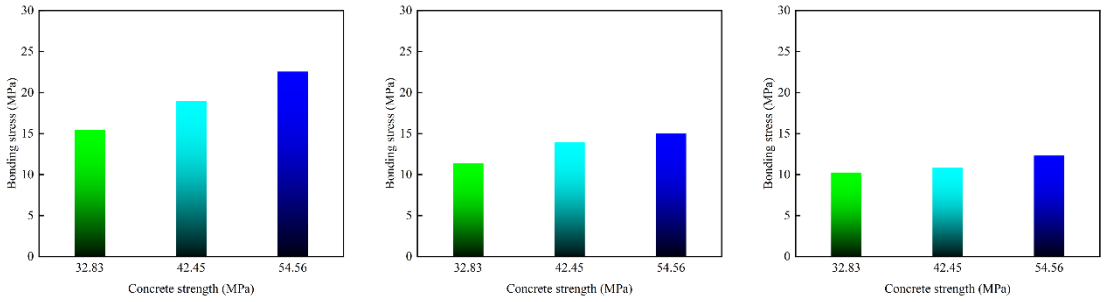

Figure13. Effect of different concrete strengths on bonding strength under monotonic load (a)Ordinary rebar(b)Carbon fiber rebar(c)Fiberglass rebar

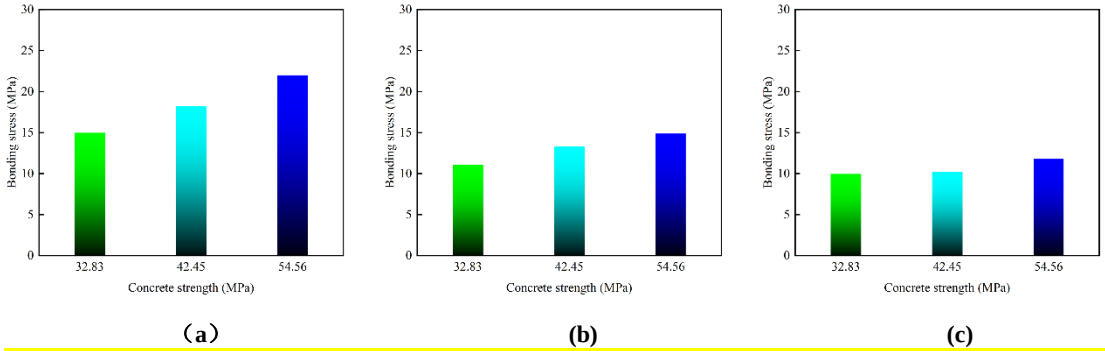

Figure14. Effect of different concrete strength on bonding strength after fatigue effect (a)Ordinary rebar(b)Carbon fiber rebar(c)Fiberglass rebar

The compressive strengths of the concrete used in this test were all close to or greater than 30 MPa on average. By comparing Fig 13(a), (b), and (c), it is found that the concrete strength has a significant effect on the bonding properties of the reinforcement. As shown in Figure 13, under monotonic loading, steel reinforcing bond strength improves by about 45.92% as concrete strength increases from C30 to C50. The bond strength of CFRP reinforcement increases by approximately 32.36%, and that of GFRP reinforcement increases by approximately 20.09%. In Figure 14, under fatigue loading, the bond strength of steel reinforcement increases by approximately 46.79% as the concrete strength increases from C30 to C50. The bond strength of CFRP reinforcement increases by approximately 33.84%, and GFRP reinforcement increases by 18.17%. Comparison with the results of Shanbo et al (2020)found that the bond strength increases with the increase of concrete

strength under the same conditions such as FRP reinforcement material. By comparing Figures 13 and 14, it is observed that the variation trend of bond strength under fatigue loading is similar to that under monotonic loading, where the bond strength increases with the increase in concrete strength. By comparing Figures 13(a), 13(b), and 13(c), we can conclude that concrete strength has a greater influence on the bond performance of the reinforcement, followed by CFRP reinforcement, while the effect on GFRP reinforcement is relatively small.

The influence of concrete strength on the bond strength of FRP bars to concrete is not substantial, indicating that bond strength is not linearly related to the square root of concrete compressive strength. Increased concrete strength facilitates increased bond strength between FRP bars and concrete when other external circumstances are the same, but none of the impacts are very noticeable. This is because as the strength of concrete increases, the amount of cement increases, and the shrinkage deformation during cement setting is greater. In the FRP tendon "rib" and "rib" between the concrete on the FRP tendon rib extrusion effect is greater, the better the effect of the mechanical bite. Furthermore, when the load is applied to the FRP tendon, the extrusion between the "rib" and the concrete will occur, which will improve the compressive strength of the concrete and make the interface less likely to produce concrete crushing damage in the process of bonding and sliding damage. This effectively reduces the weakening of the mechanical bite force between the two. As a result, improving the bond between GFRP bars and concrete by increasing the strength level of concrete is not particularly useful in practice, and the input-output ratio is poor.

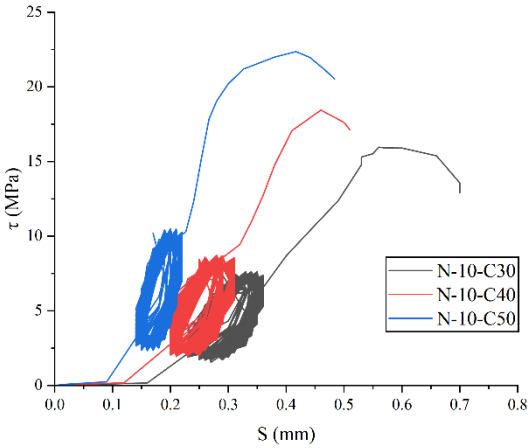

Figure15. Effect of reinforcement type on bonding performance after fatigue effect

As illustrated in Figure 15, an increase in concrete strength corresponds to a significant enhancement in the bond strength between the reinforcement and concrete. This improvement can be primarily attributed to several factors. Firstly, higher concrete strength reduces internal pore space, leading to a denser arrangement of cement paste and aggregates within the concrete. As a result, the bond between the concrete and reinforcement strengthens and becomes more stable. Under identical test conditions, fatigue loading demonstrates a tendency for the total slip of the free end of the reinforcement to decrease with an escalation in concrete strength grade. Specifically, the incremental slip between the free end of the reinforcement and the concrete for a 10 mm diameter decreases from 0.62 mm for C30 and 0.6 mm for C40 to 0.54 mm for C50. As the concrete strength increases, the total slip of the reinforcement decreases, indicating a more secure and resilient link between the reinforcement and the concrete matrix.

4.2 Effect of reinforcement diameter on bond strength

According to many domestic and foreign scholars, it was found that the influence of bar diameter on the bonding performance between FRP bars and concrete is similar to the variation rule

between steel bars and concrete, which largely shows the trend of decreasing bond stress value with increasing diameter. Therefore, this factor is considered in this paper, and the three groups of specimens with other conditions are the same, respectively. The diameter of 10 and 12 reinforced concrete specimens and their test results are shown in Figure 16 and Figure 17.

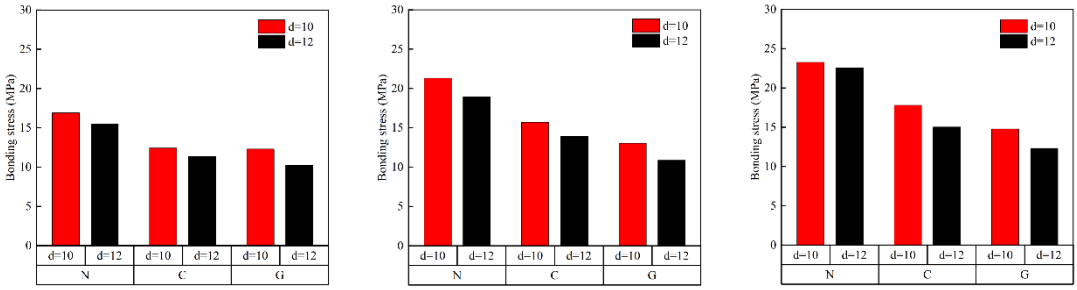

(a) **(b)** **(c)**

Figure 16. The effect of diameter on bond strength after monotonic load (a)C30(b)C40(c)C50

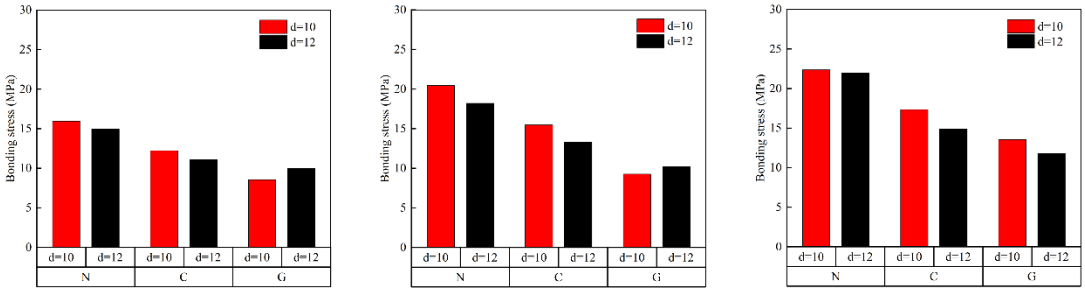

（a） **(b)** **(c)**

Figure 17. The effect of diameter on bond strength after fatigue effect (a)C30(b)C40(c)C50

The above images show that the ultimate bond between concrete and FRP tendons decreases with the increase in tendon diameter. As shown in Figure 16, taking the concrete strength of C50 as an example, under monotonic loading, the bond strengths between steel bars, CFRP bars, and GFRP bars with concrete decreased by 3.0%, 15.63%, and 16.67%, respectively, as the diameter increased from 10mm to 12mm. As shown in Figure 17, taking the concrete strength of C50 as an example, after fatigue loading, the bond stresses between steel bars, CFRP bars, and GFRP bars with concrete decreased by 1.65%, 14.19%, and 13.13%, respectively, as the diameter increased from 10mm to 12mm. Comparison with the results of Zeng et al. (2022) revealed that the bond strength decreases with the increase in the diameter of the reinforcement under the same conditions such as FRP reinforcement material and concrete strength. We found by comparing Figures 16 and Figures 17 that the trend of the bond strength with diameter after fatigue loading is similar to that of the bond strength under monotonic loading. The bond strength decreases with increasing diameter. By comparing Figures 17(a), (b), and (c), it can be observed that the bond strength of steel bars is less influenced by the diameter, while the bond strength of FRP bars is more affected by the diameter. The bond tension between FRP reinforcement and concrete lowers as the reinforcement's diameter rises, and the Poisson effect and shear hysteresis of FRP reinforcement cause this phenomenon. Because FRP bars are anisotropic materials, the strength of the longitudinal fibers determines the transverse strength, and the strength of the resin on the surface of the bars determines the longitudinal strength. When the FRP tendon is pulled, the longitudinal stress is slightly reduced by the Poisson effect, and the larger the diameter of the tendon, the more the longitudinal stress is reduced, thus affecting the magnitude of the ultimate bond strength. In addition, the shear stiffness

of FRP tendons is small, and their diameter influences the development of bond stress on the surface of FRP tendons at a certain burial length. The shear hysteresis makes the deformation between the center and the cross-sectional border of the FRP tendon when the tendon is in tension, and the positive stress in the cross-section is non-uniformly distributed, which reduces the bond stress between the tendon and the concrete. The total bonding strength of concrete and FRP bars with "ribs" diminishes as the FRP bar diameter increases.

4.3 Effect of Reinforcement type on bond strength

At present, carbon fiber reinforcement (CFRP) and glass fiber reinforcement (GFRP) are used in practical projects at home and abroad. Because each type's tensile strength and elastic modulus are different, the bonding performance between them and concrete is also different. In this paper, CFRP reinforcement, GFRP reinforcement, and steel reinforcement are considered for comparison; see Figure 18 and Figure 19.

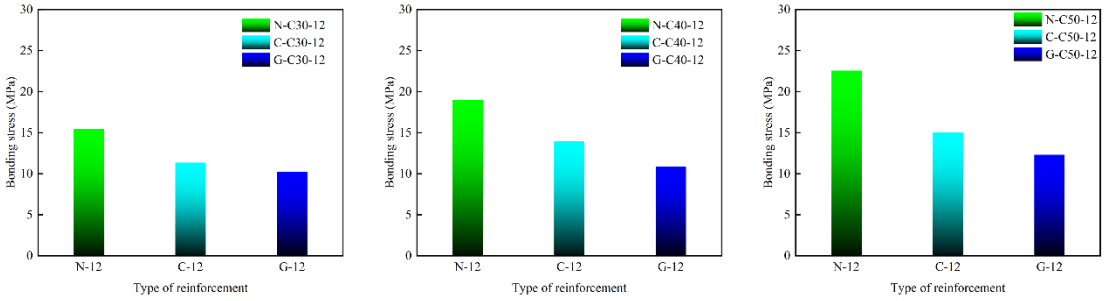

(a) **(b)** **(c)**

Figure 18. Effect of different reinforcements on bond strength monotonic load (a)C30(b)C40(c)C50

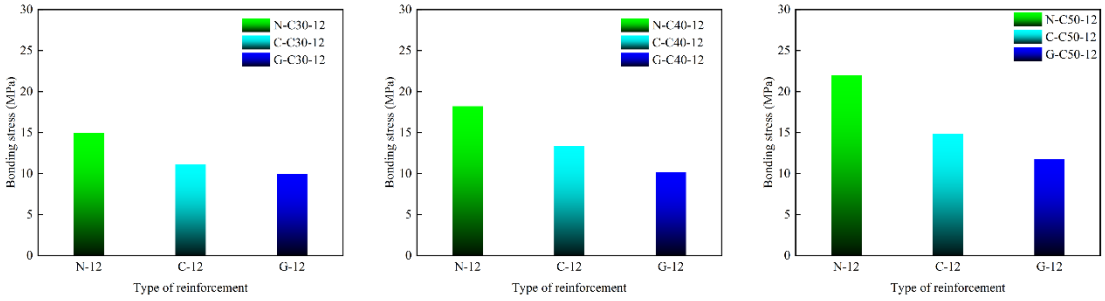

（a） **(b)** **(c)**

Figure 19. Effect of different reinforcements on bond strength after fatigue effect (a)C30(b)C40(c)C50

As can be seen in Figures 18 and 19, the bonding properties of FRP reinforcement composed of different fiber types to the concrete are different. As shown in Figure 18, taking the strength of C30 concrete as an example, the bond strength of CFRP reinforcement under monotonic loading is approximately 73.38% of the bond strength of steel reinforcement, while the bond strength of GFRP reinforcement is approximately 66.30% of the bond strength of steel reinforcement. As shown in Figure 19, taking the strength of C30 concrete as an example, the bond strength of CFRP reinforcement after fatigue loading is 74.16% of the bond strength of steel reinforcement, while the bond strength of GFRP reinforcement is 66.49% of the bond strength of steel reinforcement. Comparing Figure 18 and Figure 19, the trend of bond strength variation after fatigue loading is similar to that under monotonic loading. Both steel and CFRP reinforcements exhibit a slight decrease in bond strength after undergoing fatigue loading. This is because the fatigue cycles in this experiment were set at only 10,000 cycles, resulting in a relatively minor decrease in bond strength.

Some GFRP reinforcements showed fatigue failure in the ribs, leading to a decrease in bond strength. Therefore, it can be concluded that steel reinforcement has the best fatigue resistance, followed by CFRP reinforcement, while GFRP reinforcement has the poorest fatigue resistance.

According to the previous Figures 6 and 11, the bond-slip curves of CFRP, GFRP, and steel bars subjected to fatigue loading are comparable to their respective bond-slip curves under monotonic loading. The surface condition of the bars notwithstanding, a higher modulus of elasticity in the reinforcement material corresponds to a steeper rising section of the curve. As a result, the slope of the rising portion in the bond-slip curve of steel bars is much larger than that of CFRP and GFRP bars. It is essential to note that the reinforcement type's modulus of elasticity alone does not influence bonding performance. The surface condition of the reinforcement material also plays a crucial role. Furthermore, under the same test conditions, it is observed that a higher modulus of elasticity in the reinforcement material leads to a smaller total slip of the free end of the reinforcement after fatigue loading. The peak slip increment is also consistently larger than the residual slip increment.

In conclusion, the choice of FRP reinforcement in engineering depends on the situation. CFRP reinforcement is more expensive, so its application in civil engineering is still limited. GFRP reinforcement is the new material of choice in structural engineering due to its relatively low price and simple production.

5. Conclusions

The following conclusions can be drawn from the experiments conducted to investigate the influence of bonding properties between concrete and fiber reinforcement:

(1) As the concrete strength increases, so does the specimen's bond strength. As the concrete strength increased from C30 to C50, the reinforcement bond strength increased the most, by about 45.92%. The bond strength of the specimen of ordinary steel reinforcement is greater than that of carbon fiber than that of glass fiber. The bond strength of the carbon fiber specimen was about 70% of that of the ordinary steel specimen, while the bond strength of the glass fiber was about 60% of that of the ordinary steel specimen. The diameter of the fiberglass-reinforced concrete specimens and carbon fiber-reinforced concrete specimens had a greater effect on the bond performance. The ultimate bonding load capacity increases with diameter. Bond strength decreases with increasing diameter.

(2) The bond stress distribution along the length of the anchoring is essentially a "single peak" shape. The bond stress value will first appear near the loading end of the maximum value and from the loading end to the free end of the direction to reduce; FRP reinforcement and concrete bond will first be damaged near the loading end, the bond stress at the damage decreases, the peak bond stress will move in the direction of the free end of the bond, the bond stress along the bond length to redistribute the stress to maintain the peak bond stress to the law of diminishing returns.

(3) FRP reinforcement and concrete bond failure model includes rib shear pull-out damage, interface concrete crushing damage, and concrete splitting damage. The standard response of the axial pull-out test can be divided into micro-slip phase, slip phase, pull-out phase down phase, residual fluctuation phase, or rising section, falling section, and smooth fluctuation section. In the entire bond slip, damage between the mechanical bite between the tendon and the concrete accounted for the largest proportion.

(4) Steel bars have the highest fatigue resistance, followed by CFRP, while GFRP bars have the lowest. Comprehensive consideration, carbon fiber reinforcement not only has corrosion resistance and good fatigue resistance, and seismic performance, and high strength, high plasticity, but can effectively improve the durability of the building structure, reduce maintenance costs and extend its service life, so it is widely used in domestic and foreign marine construction projects. The fatigue resistance of glass fiber reinforcement is lower than that of carbon fiber reinforcement, and the cost is expensive, and the input-output ratio is poor.

(5) The bond-slip curves acquired through the fatigue loading mechanism are similar to those obtained through the one-way pull-out test. In fact, these curves can align and overlap across all four stages, with one notable distinction. Following fatigue loading, the peak of the bond curve is reduced, indicating a weakening of the bond strength. This reduction in bond strength can be attributed to the cumulative deformation and damage of the concrete within the bonded pull-out specimens caused by the repetitive loading action and the breakage of the reinforcement. Despite this reduction, the overall shape and behavior of the bond-slip curves remain consistent, highlighting the similarity in the bonding mechanism between fatigue loading and one-way pull-out tests.

Funding: This research was financially supported by Scientific research projects of education department of Jilin province, grant number JJKH20240381KJ; and Jilin Provincial Science and Technology Development Plan Project, grant number 20220203082SF. Natural science foundation of Guangxi 2022GXNSFAA035529. The authors wish to acknowledge the sponsors. However, any opinions, findings, conclusions and recommendations presented in this paper are those of the authors and do not necessarily reflect the views of the sponsors.

Institutional Review Board Statement:

Not applicable

Informed Consent Statement:

Not applicable

Data Availability Statement: The data used to support the findings of this study are available from the authors upon request.

Conflicts of Interest: The authors declare that they have no competing interests.

6. References

Achillides Z and Pilakoutas K (2004) Bond behavior of fiber reinforced polymer bars under direct pullout conditions. *Journal of Composites for Construction* **8(2)**: 173–181, https://doi.org/10.1061/(ASCE)1090-0268(2004)8:2(173).

Aiello MA, Leone M and Ombres L (2003) Modeling of the behavior of concrete tension members reinforced with FRP rods. *Mechanics of Composite Materials* **39(4)**: 283–292, https://doi.org/10.1023/A:1025698026124.

Benmokrane B and Tighiouart B (1996) Bond strength and load distribution of composite GFRP reinforcing bars in concrete. *ACI Materials Journal* **93(3)**: 254–259, https://doi.org/10.14359/9810.

Bowman E, Koch G, Varney J, Thompson N, Moghissi O, Gould M, et al. (2016) *International measures of prevention, application, and economics of corrosion technologies study*. NACE International, Houston, TX, USA.

Broomfield JP (2023) *Corrosion of steel in concrete*. CRC Press, London, UK.

Cosenza E, Manfredi G and Realfonzo R (1997) Behavior and modeling of bond of FRP rebars to concrete. *Journal of Composites for Construction* **1(2)**: 40–51, https://doi.org/10.1061/(ASCE)1090-0268(1997)1:2(40).

Ding Y, Ning X, Zhang Y, Pacheco-Torgal F and Aguiar JB (2014) Fibres for enhancing of the bond capacity between GFRP rebar and concrete. *Construction and Building Materials* **51**: 303–312, https://doi.org/10.1016/J.CONBUILDMAT.2013.10.089.

Edwards AD and Yannopoulos PJ (1978) Local bond-stress—slip relationships under repeated loading. *Magazine of Concrete Research* **30(103)**: 62–72, https://doi.org/10.1680/MACR.1978.30.103.62.

Huang L, Chi Y, Xu L, Chen P and Zhang A (2016) Local bond performance of rebar embedded in steel-polypropylene hybrid fiber reinforced concrete under monotonic and cyclic loading. *Construction and Building Materials* **103**: 77–92, https://doi.org/10.1016/J.CONBUILDMAT.2015.11.040.

Koch R and Balazs G (1992) Influence of preloading on bond strength and related slip. In *Proceedings of the bond in concrete-from research to practice* (American Concrete Institute (ed)). Riga, Latvia, pp. 7–11.

Koch R and Balázs GL (1993) Slip increase under cyclic and long term loads. *Otto-Graf-Journal on Research and Testing of Materialson Research and Testing of Materials* **4(1)**: 160–191.

Lindorf A and Curbach M (2010) S-N curves for fatigue of bond in reinforced concrete structures under transverse tension. *Engineering Structures* **32(10)**: 3068–3074, https://doi.org/10.1016/J.ENGSTRUCT.2010.05.025.

Lindorf A, Lemnitzer L and Curbach M (2009) Experimental investigations on bond behaviour of reinforced concrete under transverse tension and repeated loading. *Engineering Structures* **31(7)**: 1469–1476, https://doi.org/10.1016/J.ENGSTRUCT.2009.02.025.

Liu H, Yang J and Wang X (2017) Bond behavior between BFRP bar and recycled aggregate concrete reinforced with basalt fiber. *Construction and Building Materials* **135**: 477–483, https://doi.org/10.1016/J.CONBUILDMAT.2016.12.161.

Micelli F and Nanni A (2003) Tensile characterization of FRP rods for reinforced concrete structures. *Mechanics of Composite Materials* **39(4)**: 293–304, https://doi.org/10.1023/A:1025638310194.

Morita S and Kaku T (1973) Local bond stress-slip relationship under repeated loading. In *Proceedings, IABSE Symposium on the Resistance and Ultimate Deformability of Structures* (International Association for Bridge and Structural Engineering (ed)). Lisbon, Portugal, pp. 221–227.

Morita S and Kaku T (1978) Splitting bond failures of large deformed reinforcing bars. *J Am Concr Inst* **76(1)**: 93–110, https://doi.org/10.14359/6938.

Perry ES and Jundi N (1969) Pullout bond stress distribution under static and dynamic repeated loadings. *ACI Journal Proceedings* **66(5)**: 377–380, https://doi.org/10.14359/7364.

Pothisiri T and Panedpojaman P (2012) Modeling of bonding between steel rebar and concrete at elevated temperatures. *Construction and Building Materials* **27(1)**: 130–140, https://doi.org/10.1016/J.CONBUILDMAT.2011.08.014.

Rehm G and Eligehausen R (1978) Bond of ribbed bars under high cycle repeated loads. *J Am Concr Inst* **76(2)**: 76–15, https://doi.org/10.14359/6948.

Shen D, Shi X, Zhang H, Duan X and Jiang G (2016) Experimental study of early-age bond behavior between high strength concrete and steel bars using a pull-out test. *Construction and Building Materials* **113**: 653–663, https://doi.org/10.1016/J.CONBUILDMAT.2016.03.094.

Shan B, Tong G Q and Liu Q Y (2020) Experiment on bond performance of CFRP bars in seawater and sea sand concrete. *Journal of Architecture and Civil Engineering* ***37***(5): 113-123.

Tighiouart B, Benmokrane B and Gao D (1998) Investigation of bond in concrete member with fibre reinforced polymer (FRP) bars. *Construction and Building Materials* **12(8)**: 453–462, https://doi.org/10.1016/S0950-0618(98)00027-0.

Verna JR and Stelson. TE (1962) Failure of small reinforced concrete beams under repeated loads. *ACI Journal*

Proceedings **59(10)**: 1489–1504, https://doi.org/10.14359/7964.

Wu C and Chen G (2015) Unified model of local bond between deformed steel rebar and concrete: Indentation analogy theory and validation. *Journal of Engineering Mechanics* **141(10)**: 04015038, https://doi.org/10.1061/(ASCE)EM.1943-7889.0000945.

Xu YL, Shao ZM and Shen WD (1988) Bonding and anchoring strength of reinforcing steel to concrete. *Building Science* **(4)**: 10–16.

Zeng J J, Liao J, Zhuge Y, Guo Y C, Zhou J K, Huang Z H and Zhang L (2022) Bond behavior between GFRP bars and seawater sea-sand fiber-reinforced ultra-high strength concrete. *Engineering Structures*, ***254***, 113787. https://doi.org/10.1016/j.engstruct.2021.113787